Climate model forecasts of surface-level solar spectrum variation: effects on photovoltaics and crop photosynthesis

G.S. Kinsey
Zuva Energy

Abstract

Accumulation of greenhouse gases in the atmosphere alters the spectrum of sunlight that reaches the Earth's surface. Atmospheric parameters forecasted by five climate models from the Coupled Model Intercomparison Project were input to the radiative transfer model SMARTS to generate spectra over six decades (2018-2082). The potential geographic and temporal variation of photovoltaic and photosynthetic output was forecast for the spectral responses of one-, two- and three-junction PV cells, and three crop plants: corn, wheat, and rice.

Introduction

As sunlight passes through the Earth's atmosphere, it's spectrum modulated by the gases and larger particles it encounters before reaching the surface. As heat trapping from climate change accelerates, actions and interactions across the planet are shifting the atmospheric composition. The role of water vapor (as well as CO_2) to absorb solar radiation was demonstrated by Eunice Foote in 1856[1]. In addition to accumulation of carbon dioxide and increasing atmospheric pressures[2], the water content is rising due to enhanced air and water temperatures. The burning of fossil fuels produces both waste gases and particulates (aerosols). The transition towards cleaner fuels leads to a reduction in aerosols, which may be compounded by decreases in wind speeds[3].

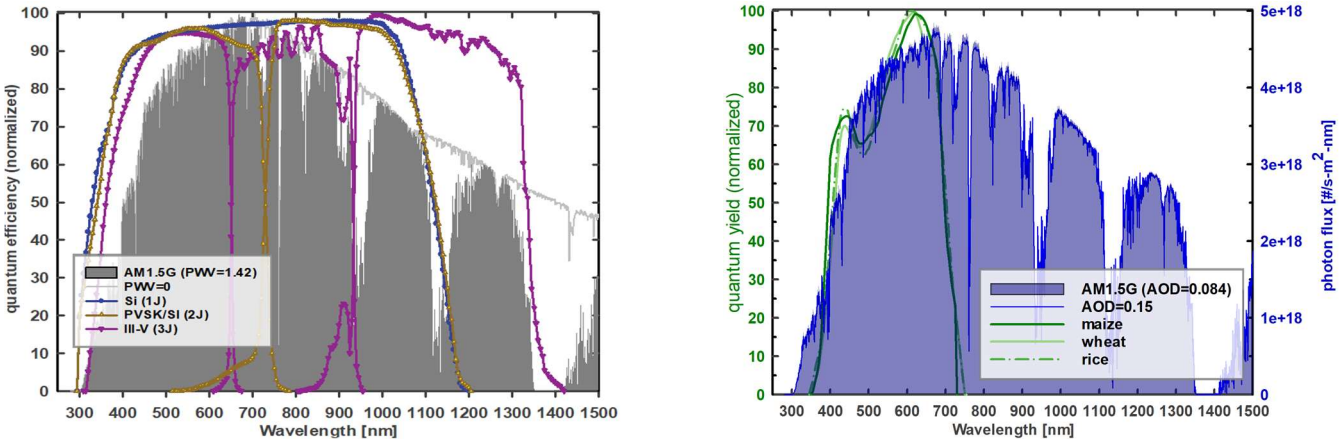

Figure 1. (a) Quantum efficiencies of a single-junction (1J) silicon (Si), tandem (2J) perovskite-silicon (PVSK/Si) and three-junction (3J) III-V multijunction cells[4–6]. The standard terrestrial solar spectrum (AM1.5G) is shown against a spectrum for which the precipitable water (PWV) has been changed from 1.42 to 0.00 [g/cm^2].
(b) Spectra of quantum yield of photosynthesis for maize, wheat, and rice[7] shown against the standard terrestrial solar spectrum (AM1.5G) and a spectrum for which the aerosol optical depth (AOD) at 550 nm has been changed from 0.084 to 0.15.

Efforts to both measure and model these trends, and their interactions, span decades[8]. The Coupled Model Intercomparison Project (CMIP) was established in 1995 to improve model accuracy and provide a knowledge base to inform international action to mitigate climate change damage. The sixth iteration (CMIP6[9]) began in 2013 and comprises 23 models which provide the underlying data for the multi-decade forecasts in reports by the Intergovernmental Panel on Climate Change (IPCC)[10]. Various future scenarios (Shared Socioeconomic Pathways, SSPs) are evaluated based on the expected level of radiative forcing from additional solar radiation being retained in the atmosphere, land, and water. The scenarios are numbered sequentially by the expected forcing by 2100: scenario 1 assumes aggressive carbon reduction and low forcing of 1.9 W/m^2 (SSP119); with continued expansion of fossil-fuel combustion, scenario 5 expects forcing to reach 8.5 W/m^2 by 2100 (SSP585). An intermediate condition considered here is scenario 2: 4.5 W/m^2 (SSP245). The effects of climate change on photovoltaics due to alterations in temperature, broadband irradiance, and cloud cover, have been studied previously[11–29]. To isolate the impact of spectrum variation, results here are taken at 25° C and normalized to the broadband irradiances.

CMIP6 models produce over a thousand parameters for forecasting changes to the geosphere. The five models selected produce the atmospheric parameters used by the radiative transfer model SMARTS to generate representative solar spectra at the Earth's surface. The parameters of interest are the aerosol optical depth at 550 nm (AOD, Figure 3), carbon dioxide, relative humidity, ozone, precipitable water (Figure 2), surface pressure (Figure 4), surface air temperature, and surface maximum temperature. Inputs were drawn from: ESM2-1 (National Centre for Meteorological Research, "CNRM"), UKESM1-0-LL (Met Office Hadley Center, "MOHC"), ES2L (Japan Agency for Marine-Earth Science and Technology, Centre for Climate System Research / National Institute for Environmental Studies "MIROC"), GISS-E2-1-G (National Aeronautics and Space Administration, "NASA"), and GFDL-ESM4 (National Oceanic and Atmospheric Administration, "NOAA"). Data was sampled once per month.

Table 1. Predicted 2020 solar cell short-circuit current relative to that under the standard spectrum (AM1.5G) at 25° C (scenario: SSP585). Currents are normalized to 1000 W/m² irradiance. "Summer"/ "winter" correspond to months 6-8/12-2 in the northern hemisphere and 12-2/6-8 in the southern hemisphere.

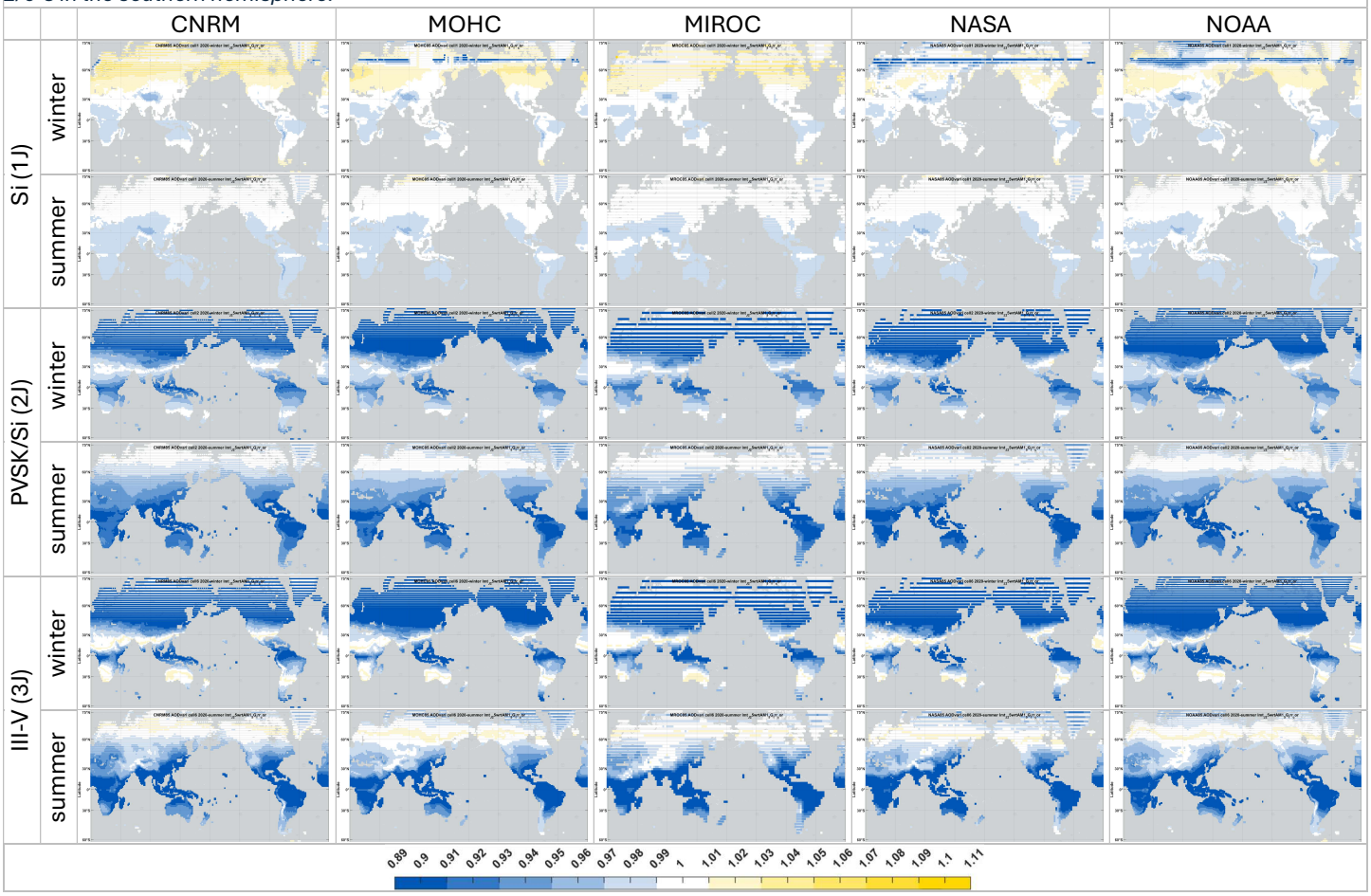

For solar cells, the spectra generated by SMARTS combined with the quantum efficiency (Figure 1a) of the solar cell gives the predicted short-circuit current of the cell. The spectral response of each cell was drawn from cells with the current-best laboratory efficiency[4–6]. An analogous process for crop plants, using the relative spectra of quantum yield of photosynthesis (Figure 1b) provides a prediction of the crop growth rates that might result when nutrient and temperature conditions are sufficient to give growth limited by the available sunlight.

Geographic variation of photovoltaic output: 2020

Using 2020 as a baseline year, the geographic distribution of photovoltaic output can be compared against the standard reference spectrum (AM1.5G). Results for the three solar cell designs are shown in Table 1. AM1.5G was established in the 1980s in the USA to represent mid-latitude (37°), fixed (non-tracking) installations. It has persisted as the go-to reference standard for laboratory efficiencies, commercial modules, and power plant performance ratings, even as PV has spread across diverse climates and tracking systems have become the backbone of utility-

scale PV energy generation. As with temperature and broadband irradiance, evaluation under more than one condition would reduce forecast errors[30,31]. Approximately 760 GW of PV was operating in 2020[32], so (assuming 1500 kWh of generation per kW of capacity) a 1% increase/decrease equates to 11 TWh of generation gained/lost, equivalent to the annual electricity consumption of the Democratic Republic of the Congo[33].

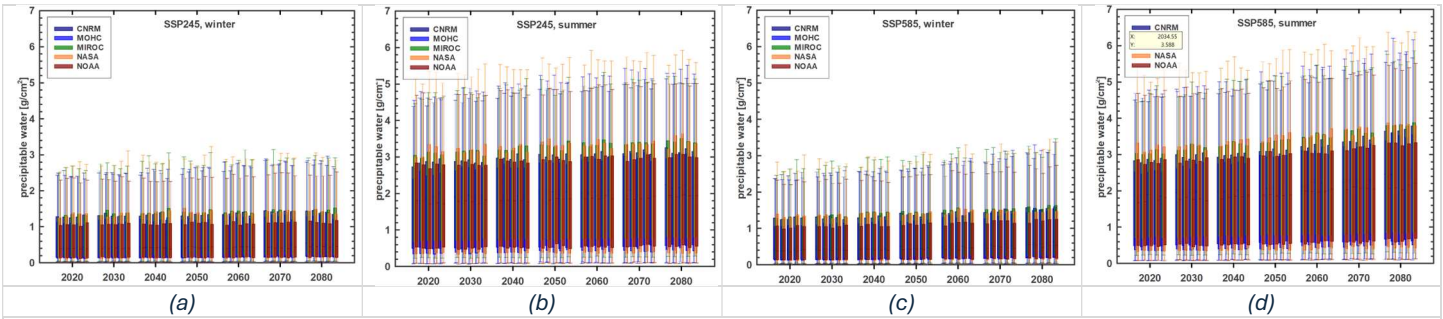

Figure 2. Precipitable water under SSP245 winter (a) & summer (b) and SSP585 winter (c) & summer (d). Winter/summer correspond to months 12-2/6-8 in the northern hemisphere and 6-8/12-2 in the southern hemisphere.

For solar cells with more than one junction, series connection of the sub-cells means that the output current is limited by whichever junction is producing the least. The resulting increase in spectrum sensitivity makes the use of a single spectrum less predictive of operating efficiency and insufficient for comparing cells with different spectrum sensitivities[30,31,34]. If a cell with more than one junction is tuned so that its sub-cell currents match under the standard spectrum, a performance peak is obtained: performance will fall off under the range of spectrum conditions found in operation. This is evident for the two-junction (2J) perovskite-silicon and the three-junction (3J) III-V multijunction cells, for which the predicted output is often more than 5% lower in latitudes below +/- 30°.

Table 2. Decadal projections of the change in seasonal short-circuit current of silicon (Si) solar cells relative to 2020 values: aerosol optical depth is held constant at 2020 values. Data is normalized by the relative irradiances.

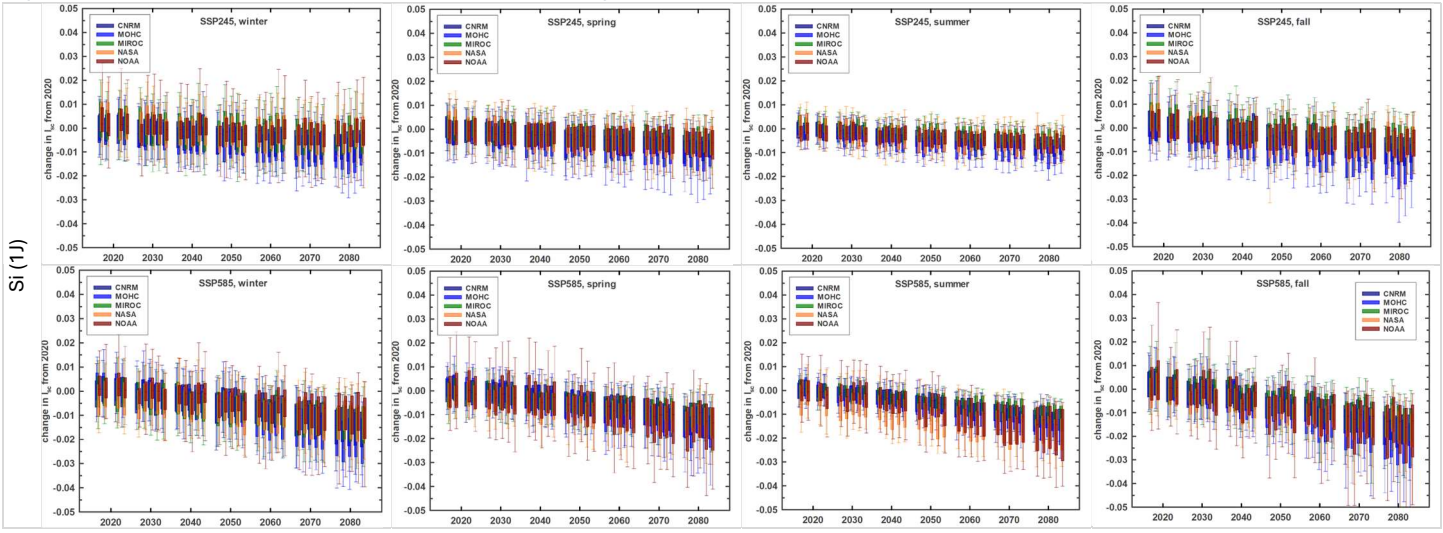

Decadal forecasts

The ability of solar PV to slow the destabilization of the climate will be altered as those changes take effect. Increases in global surface temperatures also increase evaporation and therefore the precipitable water content in the column of atmosphere above the surface[35]. The decrease in stability that results from thermal energy accumulating in the atmospheric system is expected to lead to both changes in magnitude and larger fluctuations. Absorption of radiation by water vapor occurs at wavelengths both within and beyond the absorption bands of solar cells, so the proportional impact on their outputs differs from what might be found from analysis of changes in the (broadband) solar irradiance alone. For example, the number of photons in the standard spectrum (precipitable water=1.42 g/cm^2) is about 22% lower than that of a spectrum from an atmosphere lacking water vapor (precipitable water=0 g/cm^2), Figure 1(a). The decrease within the absorption range of silicon solar cells (300-1200 nm) is 10%. The forecasts for precipitable water (PWV) are given in Figure 2. Precipitable water vapor increases with temperature, so

the downward trends in cell current over time (and between summer and winter) are expected with anthropogenic climate change[36].

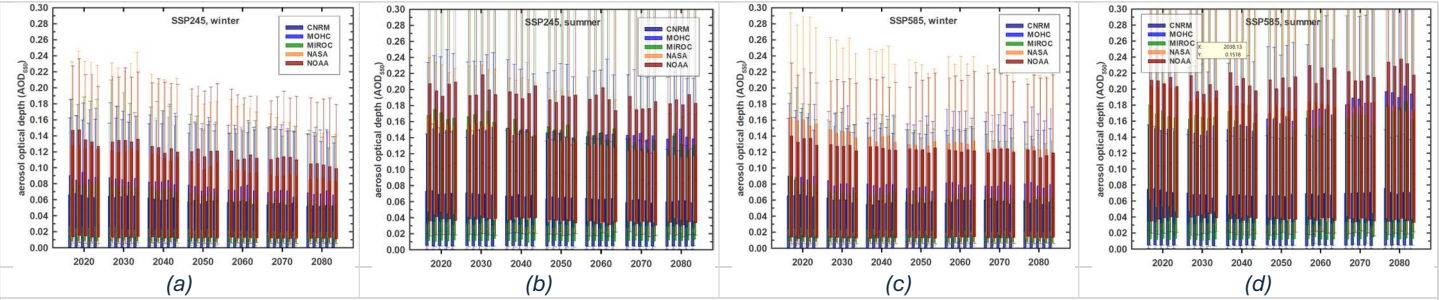

Figure 3. Aerosol optical depth at 550 nm (AOD_{550}) under SSP245 winter (a) & summer (b) and SSP585 winter (c) & summer (d). Winter/summer correspond to months 12-2/6-8 in the northern hemisphere and 6-8/12-2 in the southern hemisphere.

Table 3. Decadal projections of the change in seasonal short-circuit current of single-junction (1J) silicon solar cells relative to 2020 values. Data is normalized by the relative irradiance.

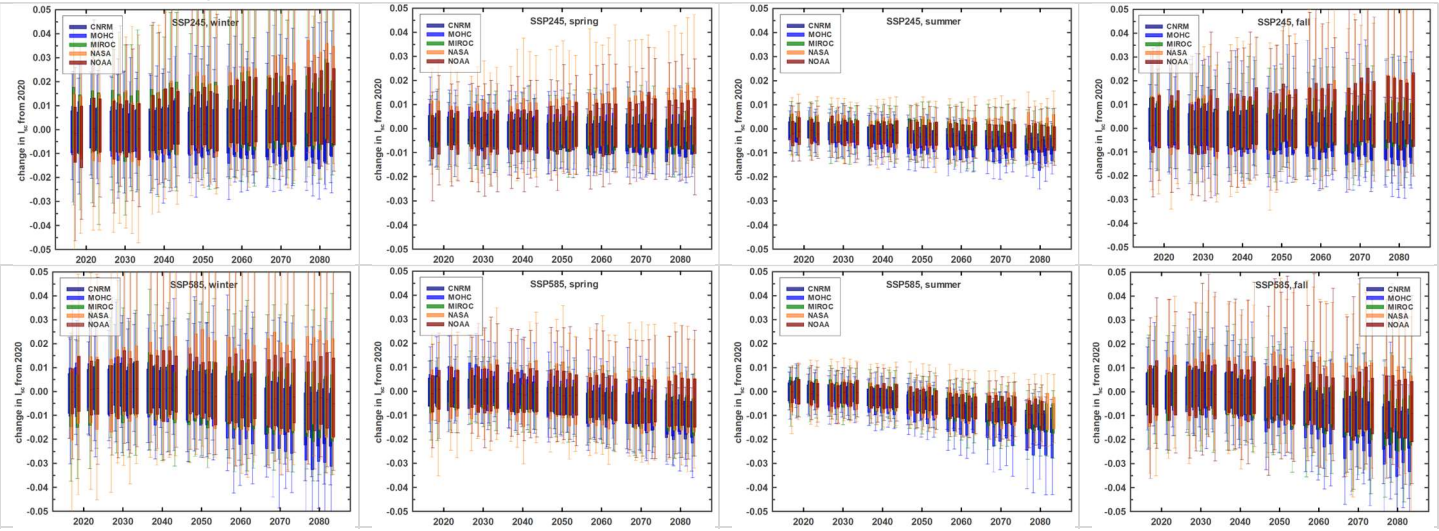

Aerosol levels in the atmosphere (quantified as aerosol optical depth, AOD) are more difficult to forecast than precipitable water vapor. Sources include fossil fuel combustion, forest fires, windborne desert dust and ocean salt, and volcanism. A patchwork approach to climate mitigation globally will give rise to both increases and decreases in aerosol levels locally and over time. While the transition from coal to natural gas (and zero-carbon sources) reduces the aerosols emitted per unit of energy, this may be more than offset by growth in total energy demand worldwide. As climate zones shift, large-scale burning of biomass may accelerate as permafrost thaws[37] and forest areas no longer contain sufficient moisture to support them[38]. Conversely, decreases in aerosols are expected from climate-change-driven reductions in wind speeds[3]. The variation in model forecasts for aerosol optical depth at 550 nm (Figure 3) reflects this uncertainty.

The forecast for solar cell short circuit currents with aerosol variation included is shown in
Table 3. With aerosol changes included, the downward trends seen in Table 2 are reduced or (for the NASA and NOAA models in fall/winter) reversed.

Table 4. Silicon (1J) short-circuit current in 2050, relative to 2020 (SSP585). (The step change seen at high latitudes in winter is due to a decline in the number of values averaged (from three to two), when the sun is below the horizon.)

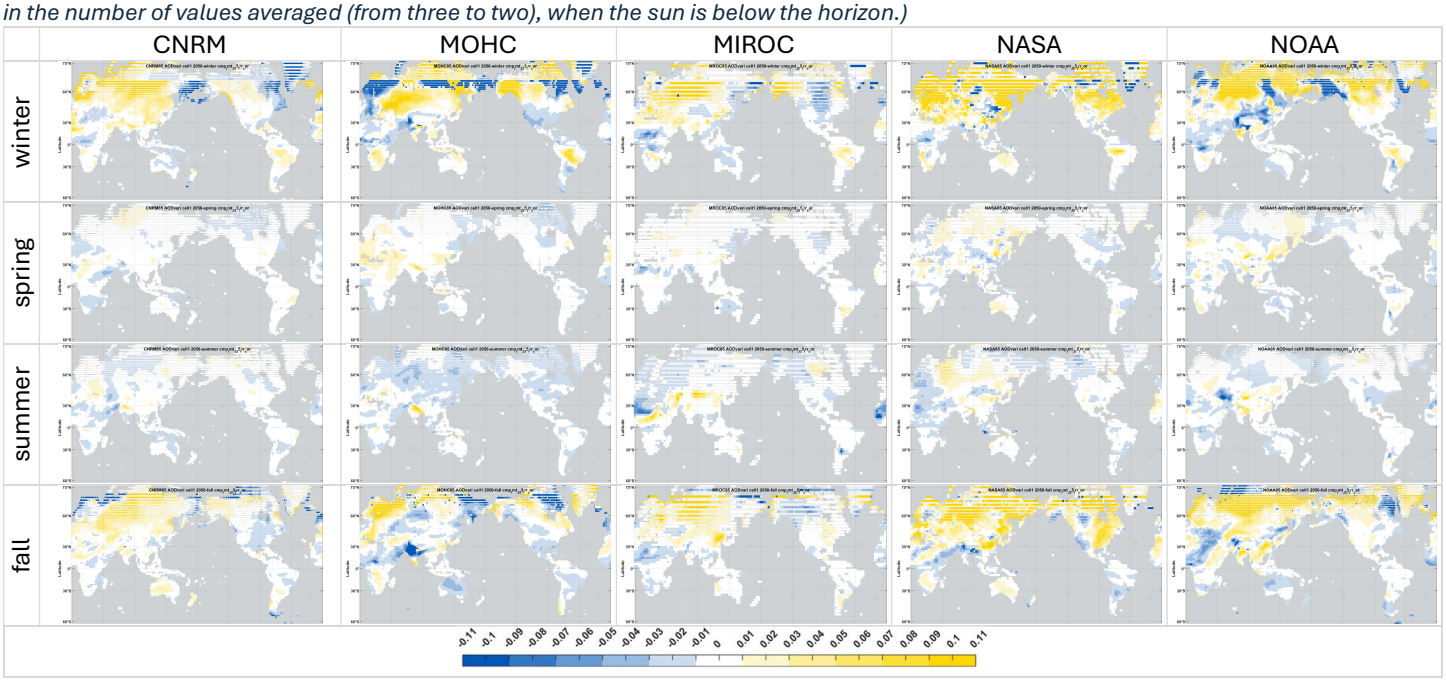

Effect on photosynthesis

For plants, an analogous metric to the quantum efficiency of solar cells is the spectrum of quantum yield of photosynthesis[7]. Integrating across the "action spectrum" (the range of wavelengths that drive photosynthesis reactions) gives the quantum yield, a measure of the efficiency at which photon energy is absorbed and converted to chemical energy via fixation of carbon. Figure 1(b) shows normalized spectra of quantum yields for three widely distributed commercial crops[7]. Borrowing the concept of a standard spectrum from PV provides a sense of the global variation in the rate of photosynthesis from these crops. The relative quantum yield of photosynthesis for maize predicted for 2020 is shown in Table 5. The absorption of plant pigments such as chlorophylls and carotenoids cuts off beyond ~700 nm, so is largely unaffected by variations in atmospheric water vapor.

Table 5. Predicted 2020 quantum yield of photosynthesis for maize, relative to that under the standard spectrum (AM1.5G), for scenario SSP585. Data is normalized to 1000 W/m^2 irradiance. "Winter"/ "spring" /"summer"/"fall" correspond to months 12-2/3-5/6-8/9-11 in the northern hemisphere and 6-8/9-11/12-2/3-5 in the southern hemisphere.

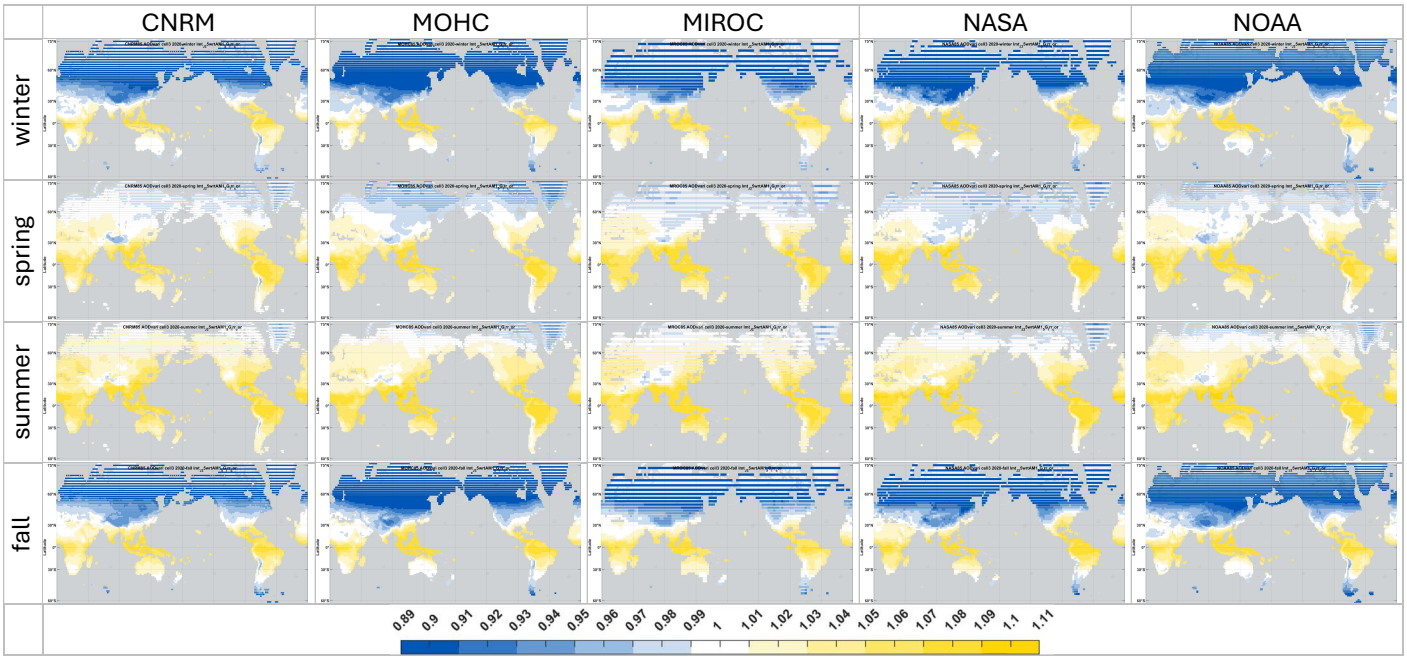

The change in quantum yield of photosynthesis for maize in 2050, relative to 2020 is shown in Table 6. The results for wheat and rice are found in the Supplemental Materials (Table 11 & Table 12).

Table 6. Maize quantum yield of photosynthesis in 2050, relative to 2020, scenario SSP585. (The step change seen at high latitudes in winter is due to a reduction in the number of values averaged (from three to two), when the sun falls below the horizon.)

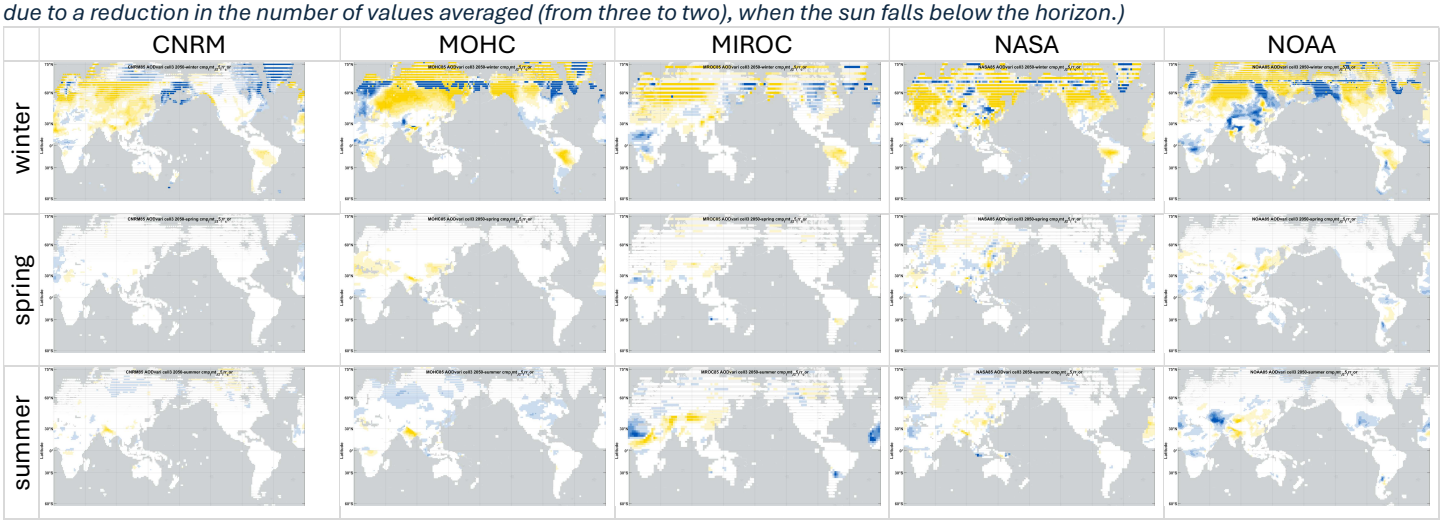

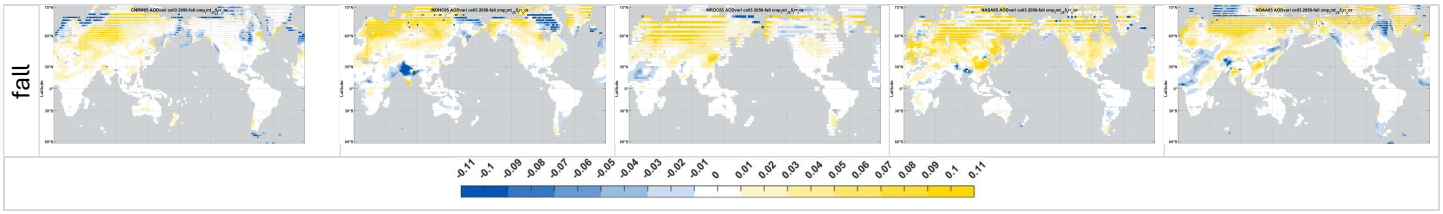
fall
Latitude
-0.11
-0.1
-0.09
-0.08
-0.07
-0.06
-0.05
-0.04
-0.03
-0.02
-0.01
0
0.01
0.02
0.03
0.04
0.05
0.06
0.07
0.08
0.09
0.1
0.11

Supplemental Materials

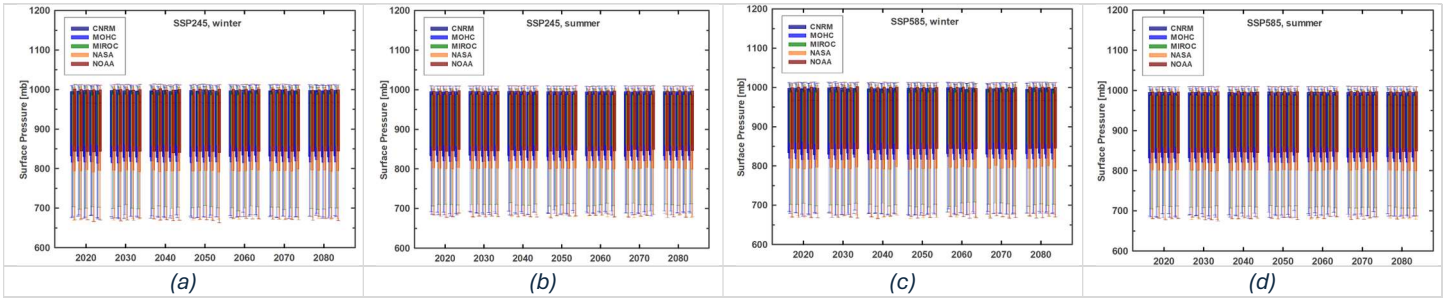

Figure 4. Surface atmospheric pressure under SSP245 winter (a) & summer (b) and SSP585 winter (c) & summer (d). Winter/summer correspond to months 12-2/6-8 in the northern hemisphere and 6-8/12-2 in the southern hemisphere.

Table 7. Decadal projections of the change in seasonal short-circuit current of tandem (2J) perovskite-silicon (PVSK/Si) and three-junction (3J) III-V multijunction (III-V) solar cells relative to 2020 values: aerosol optical depth is held constant at 2020 values. Data is normalized by the relative irradiances.

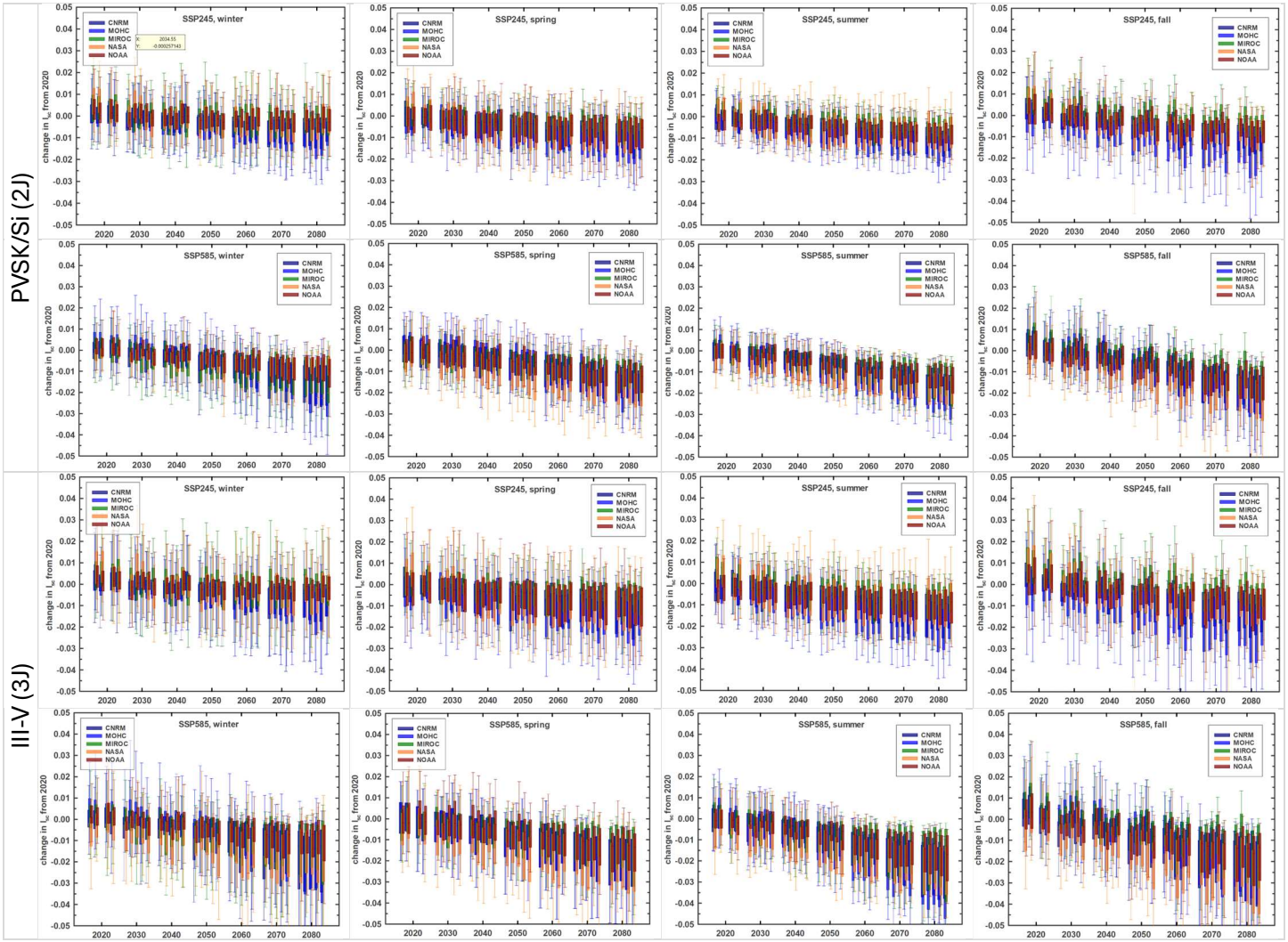

Table 8. Decadal projections of the change in seasonal short-circuit current of perovskite/silicon (2J) and III-V (3J) solar cells relative to 2020 values. Data is normalized by the relative irradiance.

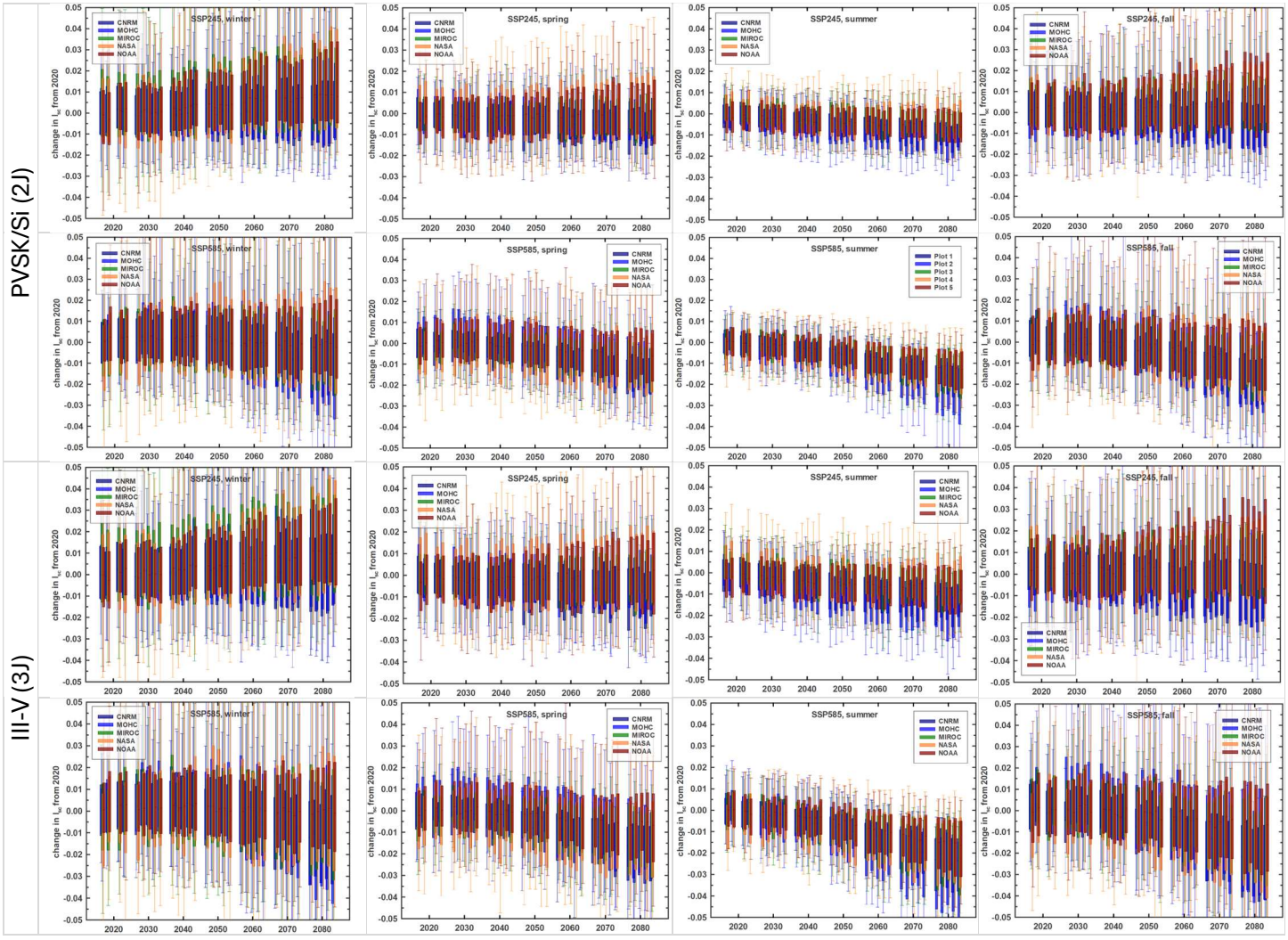

Table 9. PVSK/Si (2J) short-circuit current in 2050, relative to 2020 (SSP585). (The step change seen at high latitudes in winter is due to a reduction in the number of values averaged (from three to two), when the sun falls below the horizon.)

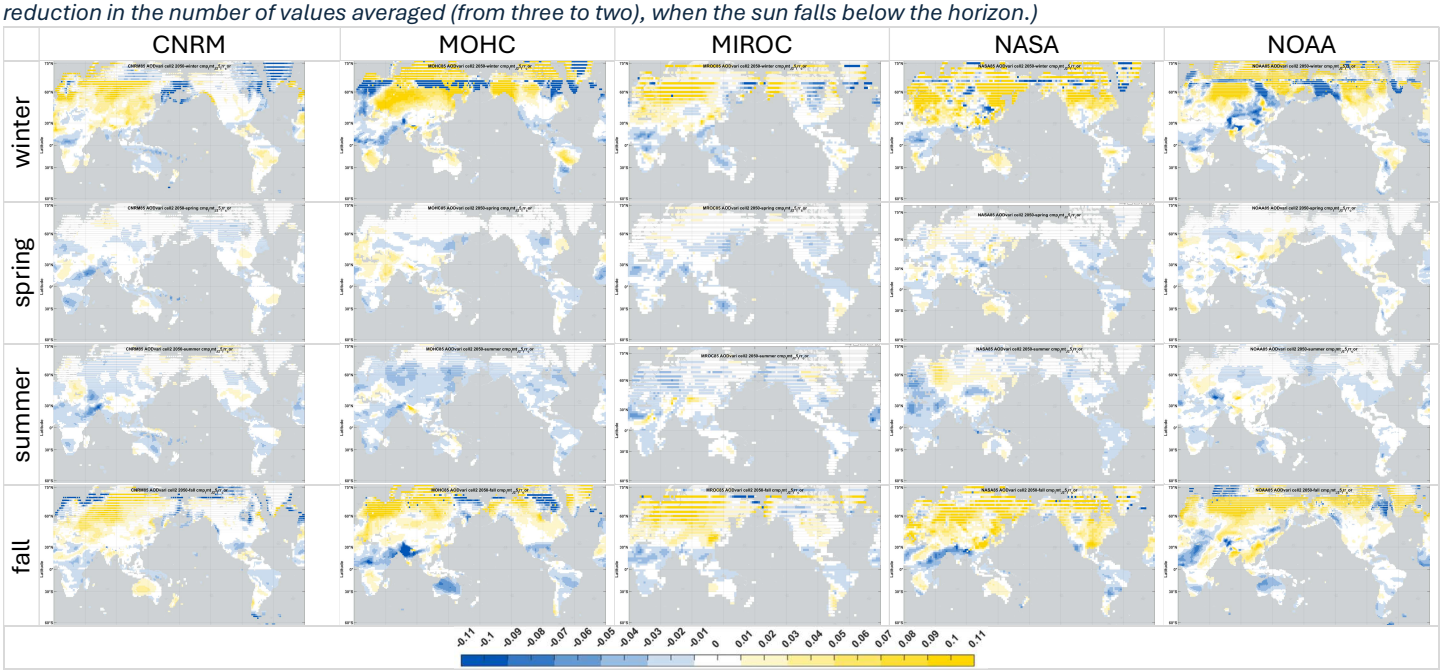

Table 10. III-V (3J) short-circuit current in 2050, relative to 2020 (SSP585). (The step change seen at high latitudes in winter is due to a reduction in the number of values averaged (from three to two), when the sun falls below the horizon.)

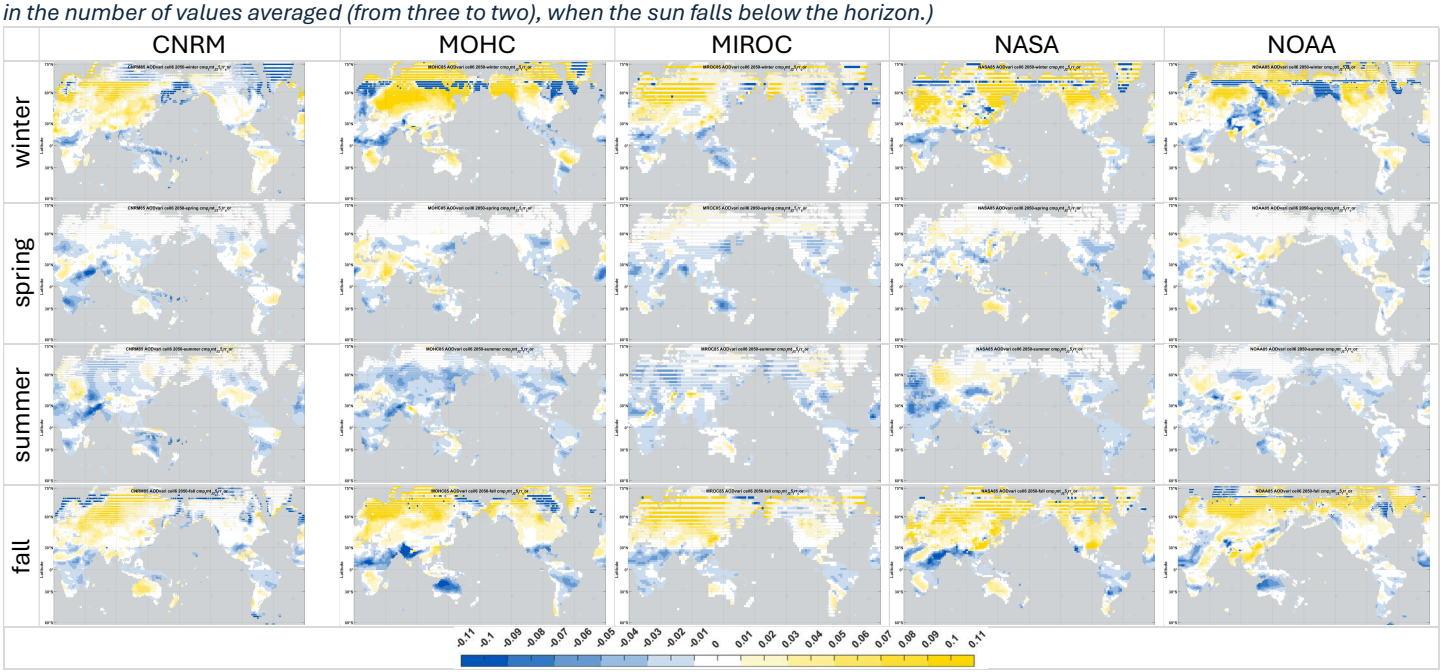

Table 11. Wheat quantum yield of photosynthesis in 2050, relative to 2020, scenario SSP585. (The step change seen at high latitudes in winter is due to a reduction in the number of values averaged (from three to two), when the sun falls below the horizon.)

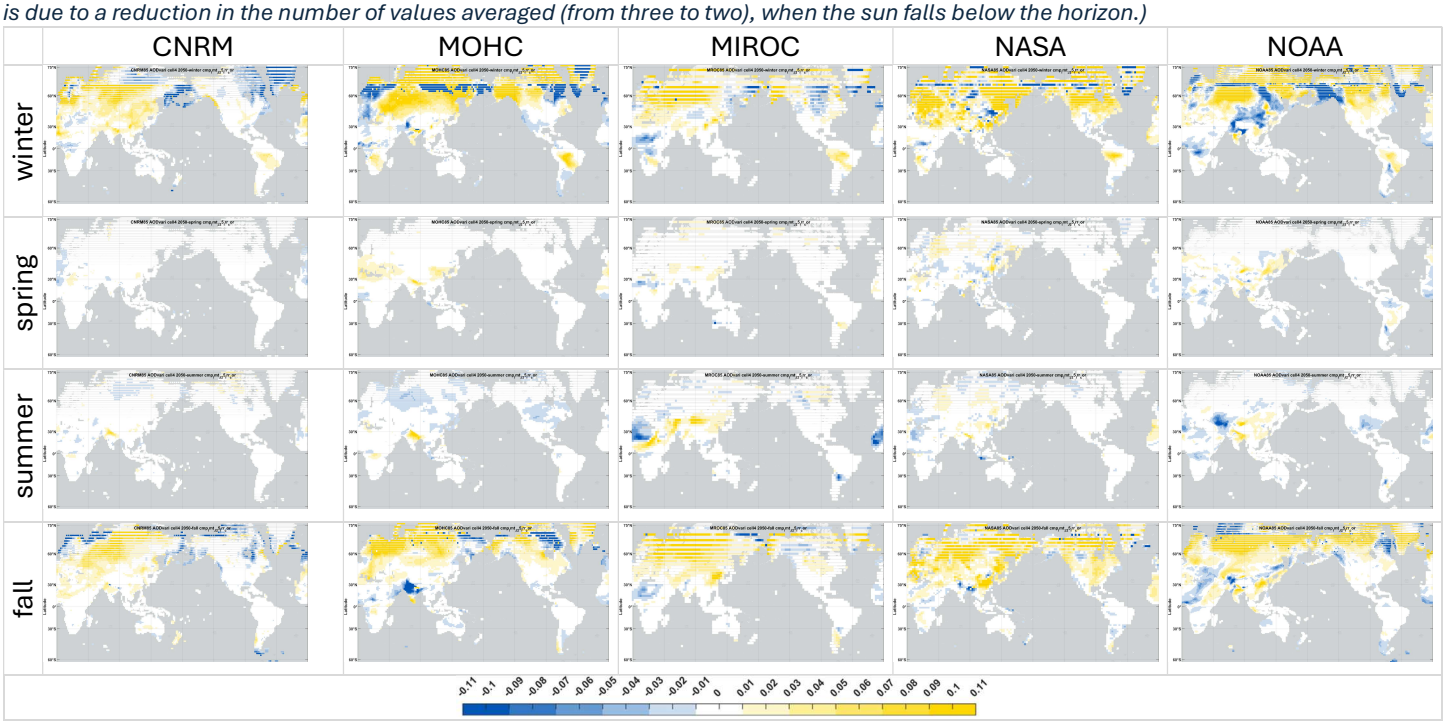

Table 12. Rice quantum yield of photosynthesis in 2050, relative to 2020, scenario SSP585. (The step change seen at high latitudes in winter is due to a reduction in the number of values averaged (from three to two), when the sun falls below the horizon.)

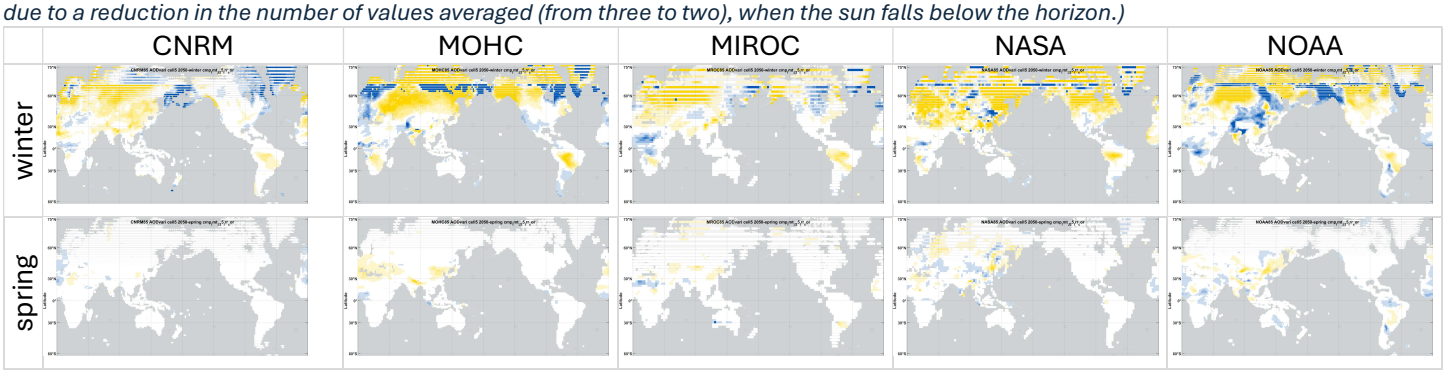

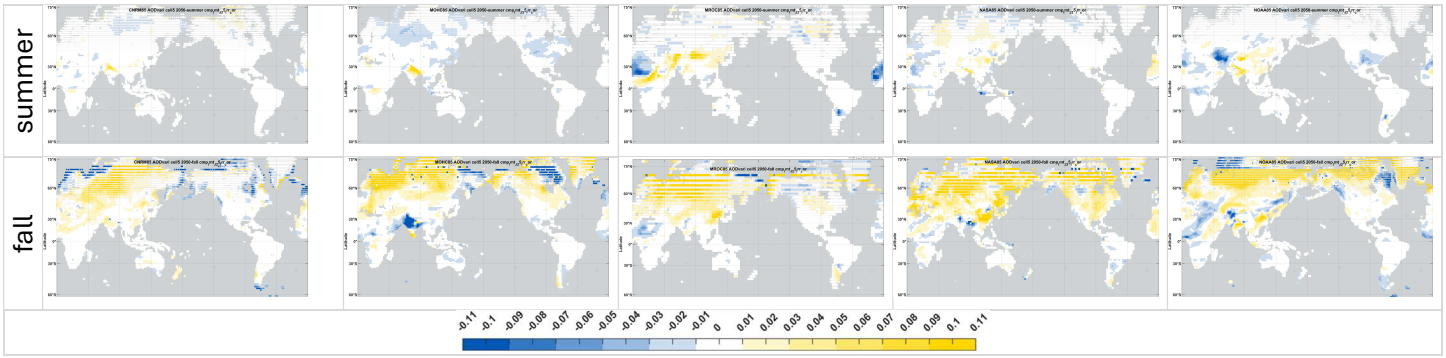
summer
fall
-0.11
-0.1
-0.09
-0.08
-0.07
-0.06
-0.05
-0.04
-0.03
-0.02
-0.01
0
0.01
0.02
0.03
0.04
0.05
0.06
0.07
0.08
0.09
0.1
0.11

References

1. Foote, E. Circumstances affecting the heat of the Sun's rays: Art. XXXI. *The American Journal of Science and Arts* 382–383 https://ia800802.us.archive.org/4/items/mobot31753002152491/mobot31753002152491.pdf (1856).

2. Gillett, N. P., Zwiers, F. W., Weaver, A. J. & Stott, P. A. Detection of human influence on sea-level pressure. *Nature 2003 422:6929* **422**, 292–294 (2003).

3. Ren, D. Effects of global warming on wind energy availability. *Journal of Renewable and Sustainable Energy* **2**, (2010).

4. Green, M. A. *et al*. Solar cell efficiency tables (version 59). *Progress in Photovoltaics: Research and Applications* **30**, 3–12 (2022).

5. Green, M. A. *et al*. Solar cell efficiency tables (Version 61). *Progress in Photovoltaics: Research and Applications* **31**, 3–16 (2023).

6. Green, M. A. *et al*. Solar cell efficiency tables (Version 63). *Progress in Photovoltaics: Research and Applications* **32**, 3–13 (2024).

7. McCree, K. J. The action spectrum, absorptance and quantum yield of photosynthesis in crop plants. *Agricultural Meteorology* **9**, 191–216 (1971).

8. Le Treut, H. *et al*. Historical Overview of Climate Change Science Coordinating Lead Authors: Lead Authors: Contributing Authors: This chapter should be cited as. (2007).

9. CMIP6: the next generation of climate models explained - Carbon Brief. https://www.carbonbrief.org/cmip6-the-next-generation-of-climate-models-explained/.

10. Intergovernmental Panel on Climate Change (IPCC). Synthesis Report — IPCC. https://www.ipcc.ch/ar6-syr/.

11. Pan, Z., Segal, M., Arritt, R. W. & Takle, E. S. On the potential change in solar radiation over the US due to increases of atmospheric greenhouse gases. *Renew Energy* **29**, 1923–1928 (2004).

12. Bartók, B. Changes in solar energy availability for south-eastern Europe with respect to global warming. *Physics and Chemistry of the Earth, Parts A/B/C* **35**, 63–69 (2010).

13. Jerez, S. *et al*. The impact of climate change on photovoltaic power generation in Europe. *Nature Communications 2015 6:1* **6**, 1–8 (2015).

14. Schaeffer, R. *et al*. Energy sector vulnerability to climate change: A review. *Energy* **38**, 1–12 (2012).

15. Gaetani, M. *et al*. The near future availability of photovoltaic energy in Europe and Africa in climate-aerosol modeling experiments. *Renewable and Sustainable Energy Reviews* **38**, 706–716 (2014).

16. Bloomfield, H. C. *et al*. Quantifying the sensitivity of european power systems to energy scenarios and climate change projections. *Renew Energy* **164**, 1062–1075 (2021).

17. Gernaat, D. E. H. J. *et al*. Climate change impacts on renewable energy supply. *Nat Clim Chang* **11**, 119–125 (2021).

18. Jaxa-Rozen, M. & Trutnevyte, E. Sources of uncertainty in long-term global scenarios of solar photovoltaic technology. *Nat Clim Chang* **11**, 266–273 (2021).

19. Feron, S., Cordero, R. R., Damiani, A. & Jackson, R. B. Climate change extremes and photovoltaic power output. *Nat Sustain* **4**, 270–276 (2021).

20. Yin, J., Molini, A. & Porporato, A. Impacts of solar intermittency on future photovoltaic reliability. *Nature Communications 2020 11:1* **11**, 1–9 (2020).

21. Kozarcanin, S., Liu, H. & Andresen, G. B. 21st Century Climate Change Impacts on Key Properties of a Large-Scale Renewable-Based Electricity System. *Joule* **3**, 992–1005 (2019).

22. Ohunakin, O. S., Adaramola, M. S., Oyewola, O. M., Matthew, O. J. & Fagbenle, R. O. The effect of climate change on solar radiation in Nigeria. *Solar Energy* **116**, 272–286 (2015).

23. Huber, I. *et al*. Do climate models project changes in solar resources? *Solar Energy* **129**, 65–84 (2016).

24. Burnett, D., Barbour, E. & Harrison, G. P. The UK solar energy resource and the impact of climate change. *Renew Energy* **71**, 333–343 (2014).

25. Panagea, I. S., Tsanis, I. K., Koutroulis, A. G. & Grillakis, M. G. Climate change impact on photovoltaic energy output: The case of Greece. *Advances in Meteorology* **2014**, (2014).

26. Ghanim, M. S. & Farhan, A. A. Projected patterns of climate change impact on photovoltaic energy potential: A case study of Iraq. *Renew Energy* **204**, 338–346 (2023).

27. Crook, J. A., Jones, L. A., Forster, P. M. & Crook, R. Climate change impacts on future photovoltaic and concentrated solar power energy systems. *Energy Environ Sci* **4**, 3101–3109 (2011).

28. Patt, A., Pfenninger, S. & Lilliestam, J. Vulnerability of solar energy infrastructure and output to climate change. *Clim Change* **121**, 93–102 (2013).

29. Pašičko, R., Branković, Č. & Šimić, Z. Assessment of climate change impacts on energy generation from renewable sources in Croatia. *Renew Energy* **46**, 224–231 (2012).

30. Kinsey, G. S. Solar cell efficiency divergence due to operating spectrum variation. *Solar Energy* **217**, 49–57 (2021).

31. Kinsey, G. S. *et al*. Impact of measured spectrum variation on solar photovoltaic efficiencies worldwide. *Renew Energy* (2022) doi:10.1016/J.RENENE.2022.07.011.

32. Snapshot 2021 - IEA-PVPS. https://iea-pvps.org/snapshot-reports/snapshot-2021/.

33. Electricity consumption by country, around the world | TheGlobalEconomy.com. https://www.theglobaleconomy.com/rankings/electricity_consumption/.

34. Kinsey, G. S. Spectrum sensitivity, energy yield, and revenue prediction of PV modules. *IEEE J Photovolt* (2015) doi:10.1109/JPHOTOV.2014.2370256.

35. Chen, B. & Liu, Z. Global water vapor variability and trend from the latest 36 year (1979 to 2014) data of ECMWF and NCEP reanalyses, radiosonde, GPS, and microwave satellite. *Journal of Geophysical Research: Atmospheres* **121**, 11,442-11,462 (2016).

36. Ren, D., Wang, Y., Wang, G. & Liu, L. Rising trends of global precipitable water vapor and its correlation with flood frequency. *Geod Geodyn* **14**, 355–367 (2023).

37. Kim, I. W. *et al*. Abrupt increase in Arctic-Subarctic wildfires caused by future permafrost thaw. *Nature Communications 2024 15:1* **15**, 1–11 (2024).

38. Barkhordarian, A., Saatchi, S. S., Behrangi, A., Loikith, P. C. & Mechoso, C. R. A Recent Systematic Increase in Vapor Pressure Deficit over Tropical South America. *Scientific Reports 2019 9:1* **9**, 1–12 (2019).